Understanding the unusual reorganization of the nanostructure of a dark conglomerate phase

M. Nagaraj,[1,*] J. C. Jones,[1,2] V. P. Panov,[1] H. Liu,[1] G. Portale,[3] W. Bras,[3] and H. F. Gleeson[1,2]
[1]*School of Physics and Astronomy, University of Manchester, Manchester M13 9PL, United Kingdom*
[2]*School of Physics and Astronomy, University of Leeds, Leeds LS2 9JT, United Kingdom*
[3]*DUBBLE Beamline, ESRF, Grenoble 38043, France*
(Received 22 January 2015; published 14 April 2015)

The dark conglomerate (DC) phase exhibited by a bent-core liquid crystal shows remarkable properties including an electric-field tunable chiral domain structure and a large (0.045) reduction of refractive index, while maintaining an optically dark texture when observed under crossed polarizers. A detailed investigation of the system is presented, leading to a model that is fully consistent with the experimental observations. It reports the observation of two distinct regimes in the DC phase: a higher temperature regime in which the periodicity measured by small angle x-ray scattering decreases slightly (0.5%) and a lower temperature regime where it increases considerably (16%). Also, the paper discusses the unusual electric-field-induced transformations observed in both the regimes. These changes have threshold fields that are both temperature and frequency dependent, though the phenomena are observed irrespective of device thickness, geometry, and the alignment layer. The electro-optic behavior in the DC phase corresponds to a number of structural changes leading to unusual changes in physical properties including a small (1%) increase in periodicity and a doubling of the average dielectric permittivity. We propose a model of the DC phase where in the ground state the nanostructure of the phase exhibits an anticlinic antiferroelectric organization. Under an electric field, it undergoes a molecular rearrangement without any gross structural changes leading to an anticlinic ferroelectric order while keeping the overall sponge-like structure of the DC phase intact.

DOI: 10.1103/PhysRevE.91.042504 PACS number(s): 61.30.Gd, 64.70.mj, 64.60.qe

I. INTRODUCTION

Very recently, we reported a dark conglomerate sponge-like phase formed from *achiral* bent-core molecules that exhibits surprising physical properties including electric-field tunable chiral domains and remarkable changes in refractive index. This is an exciting discovery and the present paper discusses the mesomorphic properties, chiral symmetry breaking, unusual temperature- and electric-field-induced changes, and the unusual reorganization mechanisms that occur in the structure of the dark conglomerate phase corresponding to these changes, and aims to produce a model consistent with the experimental findings.

Although usually associated with rod-like or disk-like molecules, liquid crystal phases have been observed for organic molecules with a variety of different and unconventional anisotropic shapes. Among these, bent-core mesogens have been considered as one of the most fascinating classes due to their wide range of unique mesophases and unusual physical properties not exhibited in more conventional (rod-like) liquid crystals [1–3]. One such set of phases exhibited by bent-core liquid crystals (BCLCs) are optically isotropic, including the recently discovered $B4$ and the dark conglomerate (DC) phases. The discovery of these phases and the subsequent understanding of their internal structures are two of the major developments in the field of BCLCs [4–16]. A characteristic common to the DC and the $B4$ phases is spontaneous breaking of chiral symmetry that occurs even though the constituent molecules are achiral. Chiral symmetry breaking and enantioselectivity are central to understanding chirality more generally, and is important for a wide range of practical applications including drug design and organic and inorganic synthesis. Unambiguously, spontaneous chiral symmetry breaking in achiral solutes is unusual. Until 1996, spontaneous mirror symmetry breaking was only known in liquid crystals having optically active molecules. Now it has been established that BCLCs show mesophases that display spontaneous chiral superstructures and polar order even though such mesophases are formed from achiral constituents [17,18] and the origin of this optical activity has been a topic of considerable interest.

Bent-core mesogens have a strong tendency to form layer structures due to their shape anisotropy. Often, the director (the vector describing the average molecular orientation) tilts with respect to the smectic layers, forming so-called smectic-C type structures. In many cases, BCLCs also show spontaneous polar ordering coplanar to the smectic layers and in the direction perpendicular to a tilt of the major director ($\boldsymbol{n}$) with respect to the layer normal ($\boldsymbol{l}$). Even though the constituent molecules are achiral, the combination of layer structure, polar order, and tilt results in internal layer chirality in polar tilted smectic phases. In such a system, the polar vector ($\boldsymbol{b}$), layer normal ($\boldsymbol{l}$), and the tilt (θ) with respect to the layer normal of the major director ($\boldsymbol{n}$) are related by ($\frac{\boldsymbol{l}\times\boldsymbol{n}}{\sin\theta} = \pm\boldsymbol{b}$) [Fig. 1(b)]. The tilted polar smectic-C phases are denoted as SmCP phases. There are four distinct structures possible in SmCP phases, depending on whether the orientation of the tilt and the polarity of adjacent layers are parallel or antiparallel. These structures are denoted as SmC_SP_F, SmC_SP_A, SmC_AP_F, and SmC_AP_A, where synclinicity and anticlinicity and ferroelectricity and antiferroelectricity are represented by the subscripts S and F and A and A, respectively [Fig. 1(b)]. For the SmC_SP_A and SmC_AP_S phases, the chirality in each layer is equal and opposite, and so the phase structures are inherently racemic. However, there is a net chirality for the SmC_SP_F and SmC_AP_A phases [Fig. 1(b)]. In many systems, the free energy of the

*mamatha.nagaraj@manchester.ac.uk

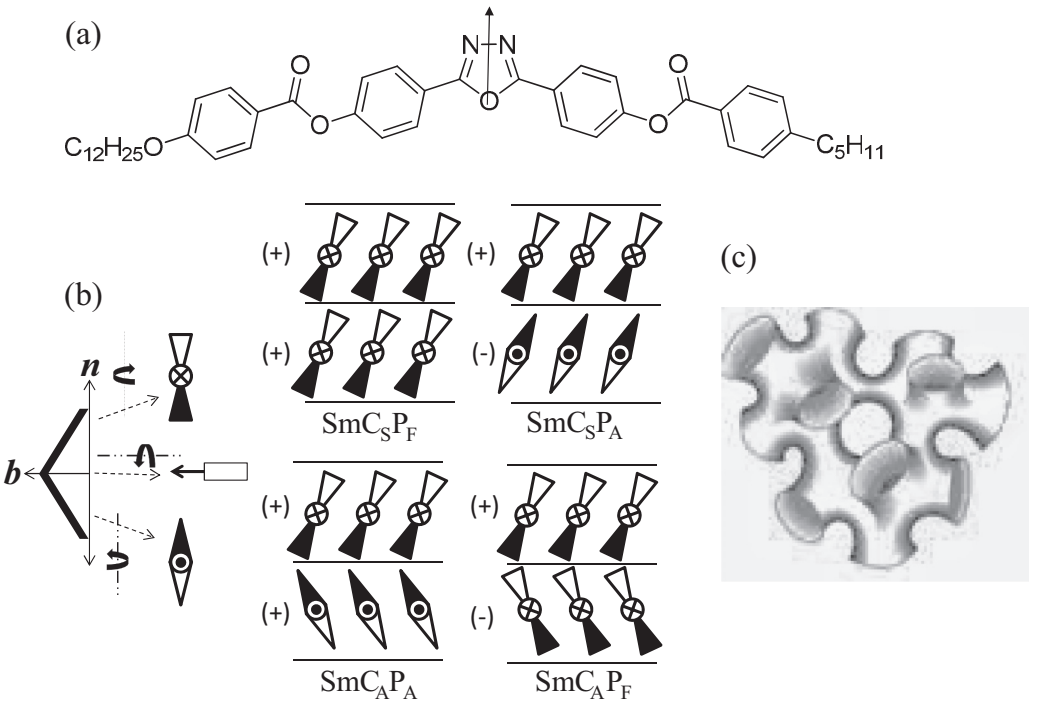

FIG. 1. (a) Molecular structure of OC12-Ph-ODBP-Ph-C5 bent-core liquid crystal; (b) cartoon representation of bent-core molecule with its major molecular director, ***n***, and the arrow direction, ***b***, and molecular arrangement in adjacent layers of SmCP phases; (d) sponge-like deformation of the layers in the dark conglomerate phases.

four structures is similar, so they can coexist at a given temperature [1,2]. Sometimes it is observed that the structures irreversibly change from one to another by the application of an electric field [1–3]. Figure 2 shows the possible molecular arrangements in the each of the SmCP phases when an electric field is applied. There are two ways to reorient the molecules; rotation around the layer normal or tilt cone (shown in red on the left-hand side in Fig. 2) and rotation around the major director (shown in red on the right-hand side in Fig. 2). Usually, only those field-induced states that preserve the total chirality of the system are observed experimentally. Both computer simulations and experimental investigations have established that BCLCs exhibit chiral conformations [19–22]. Spontaneous chiral symmetry breaking in lamellar mesophases has been attributed to either the intrinsic layer chirality or to the coupling of molecular conformational chirality to the layer chirality [20,23–25].

The DC phase, in general, is an optically isotropic phase usually found directly below the isotropic liquid or below modulated or unmodulated smectic phases. The microscopic texture of the DC phase appears completely dark or exhibits very low birefringence under crossed polarizers. On uncrossing the polarizers, the phase usually exhibits chiral domains of opposite handedness in the ground state, which is readily observed in the DC phase where there is very little or no birefringence. However, interestingly, the existence or nonexistence of the optically active domains seem to depend on the phase sequence at which the DC phase appears, with domains being visible usually when the DC phase exists immediately below the isotropic phase. The internal structure of the DC phase consists of tilted polar smectic layers (SmCP type) with relatively short interlayer correlation length and these layers curve continuously forming a saddle type structure [5], as shown schematically in Fig. 1(c). Three-dimensionally, the structure of the DC phase has significant negative Gaussian curvature and a spontaneous layer saddle splay. The in-layer frustration caused by orthogonal tilting of the molecular segments can be relieved by the saddle-splay curvature. Such a structure is analogous to the sponge structure common to lyotropic liquid crystals [26] and it is the subwavelength structure of the director formed with this spatial arrangement of the layers that makes the microscopic texture appear isotropic, and hence dark under crossed polarizers. Applying a sufficiently high electric field to the DC phase usually causes the optically isotropic DC structure to transform into a structure with synclinic and ferroelectric order (SmC_SP_F) that has long-range interlayer correlations and a simple smectic layer arrangement. That is, the applied field usually leads to the removal of the sponge-like structure and produces a highly birefringent texture under crossed polarizers [27,28].

As mentioned in the beginning of this section, we reported recently the achiral bent-core liquid crystal (OC12-Ph-ODBP-Ph-C5) based on an oxadiazole central unit that exhibits unusual mesomorphic properties in the dark conglomerate phase [29]. Interestingly, unlike the DC phase observed in other bent-core liquid crystals, the material exhibits no visible optically active domains in the ground state throughout the temperature range of the DC phase. However, when an electric field is applied, a set of unusual changes are observed. The transformation mainly involves three distinct stages. When a low field is applied across the device, the sample exhibits macroscopic conglomerates of optically active domains. As the field is increased, these domains grow continuously to give a homochiral state across the field of

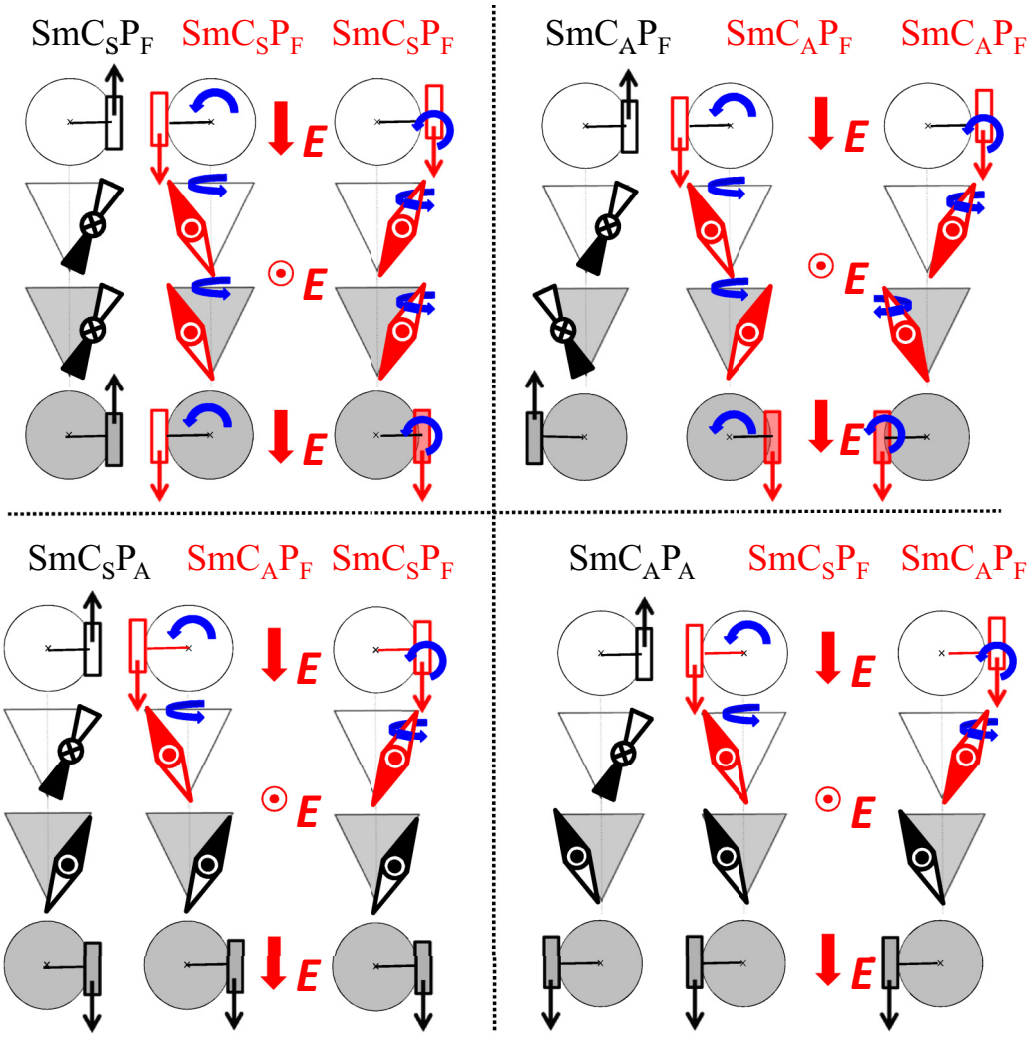

FIG. 2. (Color online) Cartoon representation of bent-core molecules around their tilt cone in various SmCP phases; in black: without electric field; in red: with electric field applied. The two possible reorientations of molecules when an electric field is applied are shown: left-hand side: rotation around the tilt cone; right-hand side: rotation around their $\boldsymbol{n}$ director.

view and finally, above a certain field, a uniform achiral state is achieved. Reference [29] provides the refractive index, circular dichroic spectroscopy, Raman spectroscopy, and current response investigations of the electric-field-induced changes in this material. To put our current results into context, we first briefly summarize these earlier findings:

(i) On increasing the applied electric field, the isotropic refractive index of the liquid crystal in the DC phase decreases from $\bar{n}$ (=1.655) to 1.61, which is close to n_o (=1.57), extrapolated from the N-DC phase transition.

(ii) Circular dichroic (CD) spectroscopy shows positive CD values for the ground state of the DC phase across its whole temperature range. The magnitude of the CD [~70 millidegrees at 350 nm] is considerably lower than is found for the DC phase for other bent-core materials. Moreover, the intensity of the CD signal decreases on increasing the applied electric field, contrary to previous findings.

(iii) Further, the Raman spectra show a peak between 1558 cm^{-1} and 1608 cm^{-1} induced upon the application of electric field. The center of this peak is at 1589 cm^{-1}, corresponding to C-C bond stretching in the phenyl rings adjacent to the center oxadiazole ring in a direction parallel to the arrow axis as labeled in Fig. 1(a). The intensity of the peak at 1589 cm^{-1} initially increases and then saturates as the field is continuously increased.

(iv) The current response of the material when the optically active domains become visible shows two current peaks per half cycle of the applied wave form. It merges into a single peak as the electric field is further increased. However, the strength of the current peaks is smaller than is reported in other DC systems when the phase transforms to lamellar phase under electric field.

The experiments on the DC phase of OC12-Ph-ODBP-Ph-C5 suggest that there could be a gross structural reorganization occurring in the DC phase when an electric field is applied. In addition, the temperature dependence of the average dielectric permittivity suggests that there are two DC phases in the system. However, no DSC peak or noticeable textural changes are observed corresponding to the DC1 to DC2 transition.

Based on the above results, we proposed a model in Ref. [29] of switching from the antiferroelectric arrangement of the layers in the ground state to the ferroelectric arrangement (switching between Sm$C_A P_A$ to Sm$C_A P_F$) under electric field without changing the tilt sense of the layers. Even though the model explained most of the experimental findings, it could not account for the unusual refractive index behavior and changes corresponding to very high electric fields. In this paper a detailed experimental study of the DC regime of OC12-Ph-ODBP-Ph-C5 was designed to allow a full understanding of both the unusual temperature- and electric-field-induced behaviors and the nature of reorganizations occurring in the dark conglomerate phase of this bent-core liquid crystal. The new experiments reported include a detailed analysis of polarizing optical microscopy textures, carried out to understand the nature of chiral symmetry breaking, together with small angle x-ray scattering (SAXS) and dielectric spectroscopy, both of which were carried out while applying high electric fields across the sample. The paper is divided into two sections. In the first section the temperature behavior of the DC phase is considered and the two apparent regimes in the DC phase investigated. In the second section electric-field-induced changes, dynamics of the chiral domains, high field SAXS, and dielectric permittivity experiments are described. The results from all of the work plus the calculation of molecular polarizability tensor are then used in the Discussion section to produce a complete model for the DC phase behavior that explains all experimental findings.

II. EXPERIMENT

The samples were formed from 1.1-mm- or 0.1-mm-thick glass etched with $1\,\mathrm{cm}^{-2}$ ITO electrodes (15 Ω/□) on opposing surfaces, onto which was deposited high temperature polyimide planar alignment layers with antiparallel rubbing. A cell spacing of 5–10 μm was defined using plastic spheres in the sealant surrounding the active area, and the device was filled with liquid crystal using capillary forces. The temperature of the sample was controlled to a relative accuracy of 0.1 K using a Linkam THMS600 hot stage connected to a T95 temperature controller. Slow cooling ($<0.5\,\mathrm{K\,min}^{-1}$) was used for all experiments. It should be noted that all of the phenomena described are independent of the alignment conditions, cooling rate, or device spacing.

An Agilent 33220A signal generator connected to a home-built amplifier was used to apply electric fields across the sample. A Leica DM2500P polarizing light microscope was used for optical observations. The images were captured simultaneously using a Deltapix Invenio 5DII camera with a 2608×1956 pixel resolution and sample size of $833 \times 666\,\mu\mathrm{m}^2$.

The small angle x-ray scattering experiments were conducted at B26B on the DUBBLE beamline at the European Synchrotron Radiation Facility (ESRF), Grenoble France. The x-ray wavelength used was 1.03 Å and the beam diameter was 0.3 mm. To enable very high temperatures and high electric fields involved in our experiments, the SAXS experiments were performed on devices prepared from ITO and polyimide coated 100-μm-thick glass plates. The samples were placed on a hot stage and mounted vertically onto the beamline [30,31].

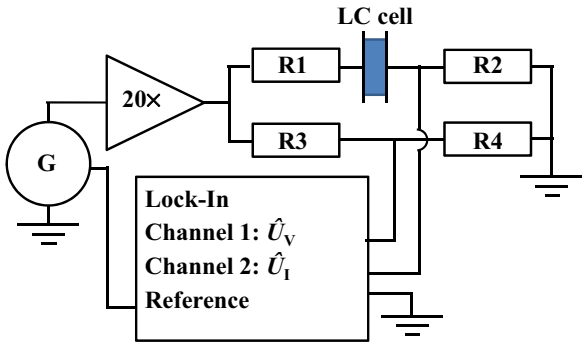

FIG. 3. (Color online) Circuit diagram of the high field dielectric setup.

The diffracted x rays from the sample were incident on a two-dimensional (2D)area detector positioned 1.4 m from the sample. Silver behenate, which has known crystalline structure and periodicity, was used for calibration [32]. The parameters of the liquid crystal such as periodicity, full width at half maximum (FWHM), and intensity and amplitude of the diffraction peaks were obtained by fitting a 2D diffraction pattern to the split-pseudo-Voigt function (SPVF).

Dielectric spectroscopy was carried out on devices with <15 Ω/□ ITO electrodes and 1.1-mm-thick glass. Figure 3 shows the circuit diagram of the high field dielectric apparatus. To measure the dielectric permittivity at high electric fields, a sine wave test voltage was applied to the liquid crystal device from the function generator via a high voltage amplifier. The current and voltage across the device were deduced from the complex voltages (V_V, V_I) measured by the two channels of the lock-in amplifier (PerkinElmer 7225 DSP). Voltage divider resistors (R_1–R_4) were used to protect the inputs of the lock-in amplifier from the high voltage test signal. The sample impedance was found from the voltages measured by the lock-in amplifier using $\hat{z}_{\mathrm{cell}} = \frac{\hat{V}_{\mathrm{cell}}}{\hat{I}_{\mathrm{cell}}}$, where $\hat{V}_{\mathrm{cell}} = \hat{V}_V \frac{R_3+R_4}{R_4} - \hat{V}_I \frac{R_1+R_2}{R_2}$ and $\hat{I}_{\mathrm{cell}} = \frac{\hat{V}_I}{R_2}$. Assuming the equivalent circuit of the LC device is a capacitance in parallel with a resistance, the real part of the dielectric constant is obtained from $\varepsilon' = \frac{1}{2\pi f C_0} \frac{-\mathrm{Im}(\hat{z})}{[\mathrm{Re}(\hat{z})^2+\mathrm{Im}(\hat{z})^2]}$ where f is the frequency of the test signal and C_0 is the capacitance of the empty device.

III. PHYSICAL PROPERTIES OF THE LIQUID CRYSTAL

The liquid crystal material studied is OC12-Ph-ODBP-Ph-C5, which exhibits the phase sequence

$$I \quad 300\,^\circ\mathrm{C} \quad N \quad 167.5\,^\circ\mathrm{C} \quad \mathrm{DC} \quad 100\,^\circ\mathrm{C} \quad \mathrm{Cry.}$$

(I: isotropic; *N*: nematic; DC: dark conglomerate; Cry: crystal phase). The molecular structure of the material is given in Fig. 1(a): OC12-Ph-ODBP-Ph-C5 is an oxadiazole based achiral BCLC and it exhibits rather unusual physical properties [29,33–40]. The nematic phase of OC12-Ph-ODBP-Ph-C5 when between untreated glass plates and observed by polarized light microscopy (POM) has spontaneous chiral domains in addition to fingerprint textures [18]. Southern *et al.* [33] employed polarized Raman spectroscopy to show that this material, in the absence of external electric or magnetic fields, exhibits nonzero values for the biaxial order parameters in

the lower temperature regime of the nematic phase. Kaur *et al.* [34] studied the electroconvection (EC) phenomena and observed unusual EC patterns in the nematic phase. The splay (K_{11}), twist (K_{22}), and bend (K_{33}) elastic constants have been measured across the entire nematic regime of this material and found to follow the relationship $K_{22} < K_{33} < K_{11}$, in common with many (but not all) BCLCs [35,36]. The temperature dependence of the splay elastic constant in the nematic phase shows a linear increase as the temperature decreases and takes values approximately twice that of equivalent compounds but with shorter alkyl terminal chains. The twist elastic constant K_{22} also increases linearly with decreasing temperature whereas K_{33} is almost temperature independent. Atomistic calculations show that the bend angle is the dominant parameter in determining the elastic behavior of a bent-core liquid crystal [36,37] and that the inequality $K_{33} < K_{11}$ is associated with the oxadiazole bend angle of ∼140°. In contrast, materials with higher bend angles give $K_{33} > K_{11}$. Moreover, the nematic phase of OC12-Ph-ODBP-Ph-C5 has much lower twist and bend elastic constants, and higher nematic flexoelectric coefficients compared to similar molecules [40]. It is the DC phase that occurs at temperatures directly below the nematic phase of this material that is of interest in this paper.

IV. RESULTS

A. Temperature behavior

The DC phase in OC12-Ph-ODBP-Ph-C5 exists over a wide range of temperature of ∼65 °C. On heating, it transforms into the nematic phase via a filament texture that exists for <0.1 °C [18]. On cooling the sample from the nematic phase, a first order transition to the DC phase is observed by polarizing optical microscopy, where the domains of the DC phase grow into the nematic phase as fractal-like domains with distinct boundaries separating the two phases. In the ground state the texture of the DC phase has a few small, achiral defect regions that are slightly birefringent. The size of these defects depends on the heating or cooling rate of the sample and they are more clearly visible in thin cells (Fig. S1, Ref. [29]). No spontaneous chiral domains are visible at any temperature in the DC phase, neither on heating nor on cooling, and the texture remains the same throughout the DC temperature range. At 100 °C, the optically isotropic DC phase becomes a crystal phase with a highly birefringent texture.

In order to gain a better insight into the internal structure of the DC phase, small angle x-ray scattering (SAXS) experiments were performed on 5–10-μm-thick planar, homogeneously aligned devices. The 2D diffraction pattern of the ground state of the DC phase shows a diffuse ring [Fig. 4(a) inset]. The measured periodicity (d) close to the N to DC phase transition is 30.1 Å (±0.001 Å), Fig. 4(a). The calculated molecular length (L) of OC12-Ph-ODBP-Ph-C5 obtained from molecular modeling is ∼34 Å [18]. Assuming that the periodicity measured by SAXS corresponds to a SmC layer spacing, the molecular tilt angle, θ_C, can be determined according to $\cos\theta_C = d/L$. Thus the periodicity close to the N to DC transition corresponds to tilted molecules with $\theta_C = 27.7°$. On reducing the temperature, the periodicity of the DC phase initially decreases to 29.95 Å (i.e., tilt increases to

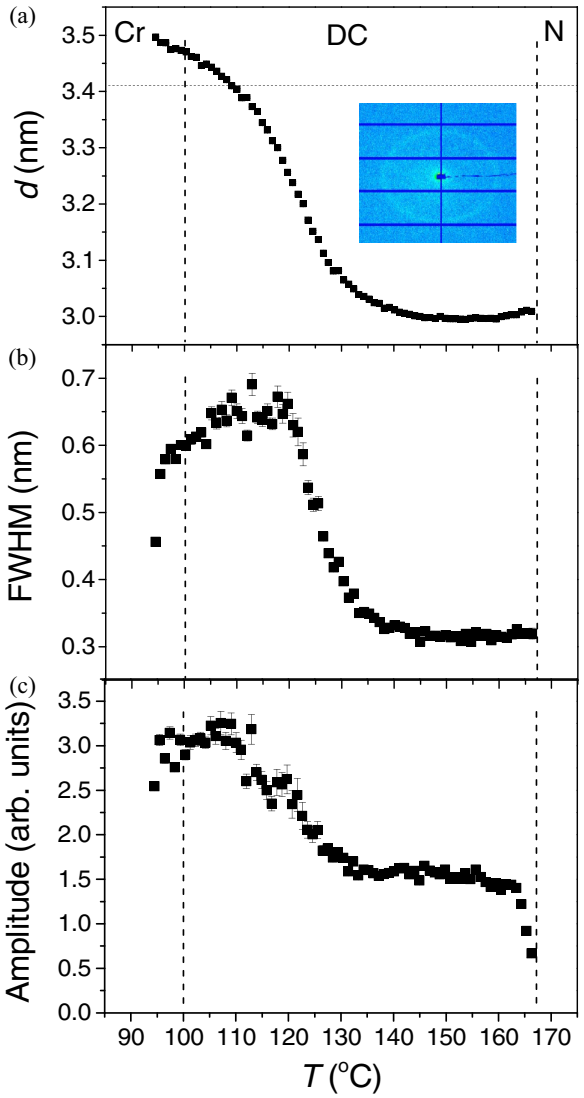

FIG. 4. (Color online) Temperature dependence of (a) periodicity, d, (b) FWHM, and (c) amplitude of the peak of OC12-Ph-ODBP-Ph-C5 liquid crystal on cooling below the N-DC phase transition temperature.

$\theta_C = 28.3°$) for a range up to $T - T_{N\text{-DC}} \sim -30$ °C [Fig. 4(a)]. This change in the d spacing over the temperature interval $0 < T - T_{N\text{-DC}} <\sim -30$ °C corresponds to a constant layer FWHM of 0.3 nm (=3.33 nm^{-1}) and a constant peak amplitude of 1.5 arb units [Figs. 4(b) and 4(c)]. On further lowering the temperature, the d spacing increases, becoming considerably higher below $T - T_{N\text{-DC}} \sim -30$ °C, and saturates at $d =$ 35 Å prior to the crystalline transition. This change in d is concurrent with a large increase of both the FWHM (from 0.3 to 0.66 nm) and a near doubling of the peak amplitude. The two regimes corresponding to two distinct behaviors in the DC phase are labeled as DC1 and DC2, with DC1 being the higher temperature regime. The d values obtained here are in good agreement with literature values obtained from bulk samples [41].

The material was investigated by dielectric spectroscopy with a weak voltage (0.1 V) applied across the sample in the

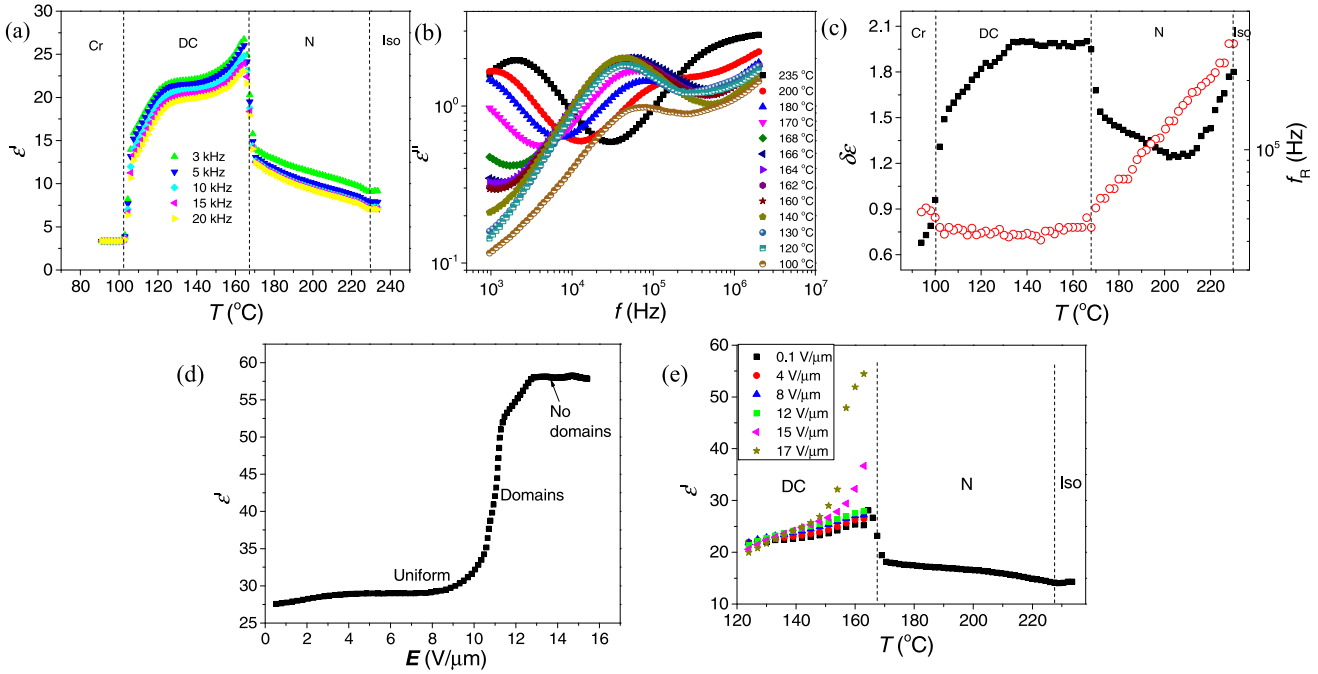

FIG. 5. (Color online) (a) Temperature dependence of the dielectric permittivity ε' for various frequencies; (b) frequency dependence of the dielectric loss ε'' for selected temperatures; (c) temperature dependence of dielectric strength, $\delta\varepsilon$, and the relaxation frequency, f_R; (d) electric-field dependence of the dielectric permittivity, ε', for $f = 1$ kHz in the DC phase at $T - T_{N\text{-DC}} = -4\,^{\circ}$C. The threshold fields corresponding to textural changes are $\boldsymbol{E}_{th1} \sim 8\,\mathrm{V}\,\mu\mathrm{m}^{-1}$ and $\boldsymbol{E}_{th2} \sim 12\,\mathrm{V}\,\mu\mathrm{m}^{-1}$. (e) Temperature dependence of the dielectric permittivity ε' for various electric fields.

frequency range between 1 kHz and 2 MHz and at temperatures between 90 °C and 235 °C on cooling. Figure 5(a) shows the temperature dependence of the dielectric permittivity, ε', of the material for selected frequencies. The data show a clear first order transition between the nematic and the DC phase, as expected. It is also clear that ε' is maximum at the N to DC transition and its value decreases by ∼20% as the sample is cooled further into the DC1 phase. The slopes of the decrease in permittivity in DC1 and DC2 regimes are different with the rate of change of permittivity being high in the DC2 regime. (The plot of ε' for various frequencies as a function of temperature was previously reported in Ref. [29]. These data showed a sudden increase in the ε' at $T - T_{N\text{-DC}} = -35\,^{\circ}$C. We attribute this sudden change in ε' to an instrumental artifact. For the data presented in this paper, necessary changes to the software have been made to allow sufficient experiment delay time to avoid such effects.) In the nematic phase, for frequencies of ∼1 kHz, $\varepsilon'_{\perp} \sim 15$ and $\varepsilon'_{\parallel} \sim 9$ implies $\bar{\varepsilon} \sim 13$, whereas in the DC phase, the measured permittivity is ∼25 close to the N-DC transition, which is higher than the $1/T$ extrapolation of $\bar{\varepsilon}$ and the measured ε in the isotropic phase. This clearly indicates that the molecular motions become collective at the N-DC phase transition, due to the polarization inherent to the phase. The plot of the imaginary part of complex dielectric permittivity, ε'', as a function of frequency for various temperatures is given in Fig. 5(b). The main feature of the graph is a relaxation mode that occurs in the middle frequency range in the entire temperature range. The plot of dielectric strength ($\delta\varepsilon$) and the relaxation frequency (f_R) of the middle frequency relaxation mode are given in Fig. 5(c). (The two distinct behaviors in the $\delta\varepsilon$ in the nematic phase will be discussed elsewhere). The $\delta\varepsilon$ increases sharply (1.5 to 2) close to the N-DC phase transition and reaches a maximum at the phase transition. Further into the DC phase, $\delta\varepsilon$ remains almost constant through the DC1 regime but starts to decrease rapidly at temperatures corresponding to the DC1 to DC2 change. The relaxation frequency (f_R) of this mode far from the N-DC phase transition decreases with decreasing temperature following the Arrhenius dependence [42] which deviates from such behavior close to the phase transition. There is no significant change in the relaxation frequency in the entire DC phase temperature range.

B. Electric-field behavior

1. *Polarizing optical microscopy*

When an electric field is applied across the DC phase at $T - T_{N\text{-DC}} = -4\,^{\circ}$C, there is no observable change of texture for fields below $8\,\mathrm{V}\,\mu\mathrm{m}^{-1}$. At $\boldsymbol{E} = \boldsymbol{E}_{th1} \sim 8\,\mathrm{V}\,\mu\mathrm{m}^{-1}$, the initial texture with low birefringence defects [Fig. 6(a)] changes to a uniformly dark texture [Fig. 6(b)] under crossed polarizers. On further increasing the field to $\sim 12\,\mathrm{V}\,\mu\mathrm{m}^{-1}$ ($=\boldsymbol{E}_{th2}$), the texture remains uniform and dark, but uncrossing the polarizers reveals tiny domains (∼5–10 μm in size) of opposite handedness [Figs. 6(c) and 6(d)]. Further continuous increase of the applied electric field causes these domains to coalesce and grow to form larger domains with smooth boundaries. Once a large domain of a particular handedness is formed, any tiny domains of the opposite handedness in its vicinity reorganize to the chiral sense of the larger domain. The dynamics of the domain growth depends on time, frequency, and the strength of the applied electric field. In other words, for a given frequency and field above $\boldsymbol{E}_{th2}$, the size of the chiral

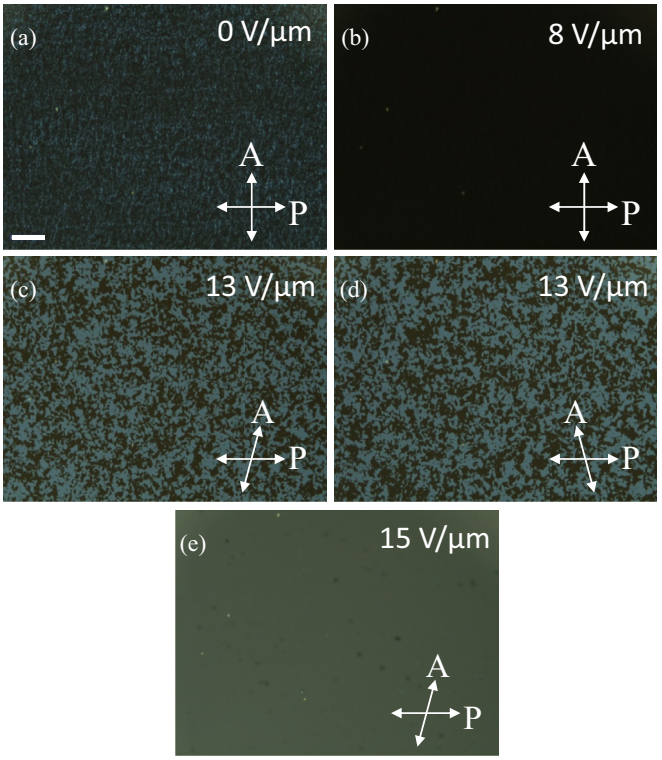

FIG. 6. (Color online) POM textures of the DC phase in a 5-μm planar cell at (a) $\boldsymbol{E} = 0$; (b) uniform dark texture at $8\,\mathrm{V}\,\mu\mathrm{m}^{-1}$, domains of opposite handedness on uncrossing the polarizers in opposite directions at (c), (d) $13\,\mathrm{V}\,\mu\mathrm{m}^{-1}$; (e) achiral texture at $15\,\mathrm{V}\,\mu\mathrm{m}^{-1}$. $f = 1$ kHz, T–$T_{N\text{-DC}} = -4\,^{\circ}$C. P and A are the polarizer and analyzer directions. Length of the white bar is 100 μm.

domains increases with time. For a given electric field changing the frequency of the applied wave form, f changes the rate of the domain growth, with the higher frequency leading to larger sized domains in the same time. A similar trend is found for increasing field for a given frequency. In each case, the domains of opposite handedness are separated by sharp interfaces that are different than the faceted [43] and curved boundaries formed for field-induced dark conglomerate phases [44] observed in other materials. Figure 7 shows POM textures of the growth of optically active domains for a continuous increase in electric field at $f = 1$ kHz (pictures are taken immediately after applying an electric field).

It is interesting that as the conglomerate domains grow, their area distribution does not remain the same, and domains of one handedness begin to dominate. This is depicted in Fig. 8(a), which describes the variation in the area occupied by the chiral domains in the field of view of the microscope, as a function of time, for $\boldsymbol{E} = 14\,\mathrm{V}\,\mu\mathrm{m}^{-1}$ and $f = 1$ kHz. The area is calculated from the histograms of the photomicrographs of the chiral domains. During these experiments, care was taken to obtain histograms having two sharp modes corresponding to low and high intensities. Also, a large area of the sample was covered (approximately 1.5 mm diameter, viewed using a 5× objective) and the data were averaged for several photographs taken from different parts of the device. The clear bias towards the growth of one handed domain over the other is further supported by the behavior of the sample at higher electric fields at which the field of view is completely occupied by one handed domain. The chiral nature of this enantiomeric state is confirmed by uncrossing the polarizers in opposite directions by the same angle, a process that reveals two distinct optical states. Remarkably, it is always the left-handed domains that dominate in all experiments conducted, irrespective of the sample spacing, alignment layers (planar or homeotropic), and the geometry of the cell (planar or twisted). During all of the described changes that occur after the chiral domains of opposite handedness become visible ($\boldsymbol{E} > \boldsymbol{E}_{\mathrm{th2}}$), the sample remains completely dark when viewed between crossed polarizers, and rotation of the cell with respect to the polarizers does not cause any change of the texture or transmitted light. Further increase of the electric field, $\boldsymbol{E} > \boldsymbol{E}_{\mathrm{th3}} = 15\,\mathrm{V}\,\mu\mathrm{m}^{-1}$ at 1 kHz, results in the disappearance of the chiral domains, leaving a uniform achiral texture across the entire field of view [Fig. 6(e)]. At this point, uncrossing the polarizers in opposite directions yields the same optical state.

As mentioned, the field-induced states occur irrespective of the type of the wave form applied (sine, square, and triangular), the sample thickness (1.6–20 μm), geometry of the device, and the alignment (planar, homeotropic, and twisted) used. Also, the transformations are seen at all temperatures corresponding to the DC phase (DC1 and DC2), whereas no change in the texture is observed for the lower temperature crystal phase even on exposure to very high electric fields ($\sim 20\,\mathrm{V}\,\mu\mathrm{m}^{-1}$). However, the threshold electric fields required to achieve these field-induced states depend on the type of the applied wave form, frequency, and the temperature. Figure 8(b) shows the frequency dependence of the three threshold electric fields for a given temperature. The thresholds $\boldsymbol{E}_{\mathrm{th1}}$ and $\boldsymbol{E}_{\mathrm{th2}}$ are independent of frequency to within error whereas $\boldsymbol{E}_{\mathrm{th3}}$ decreases as the frequency increases. This implies that above a certain frequency, for a given temperature (for example 5 kHz at $T - T_{N\text{-DC}} = -4\,\mathrm{K}$), the domains that appear above $\boldsymbol{E}_{\mathrm{th2}}$ disappear at lower fields than is observed for lower frequencies. The decrease of $\boldsymbol{E}_{\mathrm{th3}}$ as the frequency increases could be related to the conductivity anisotropy of the sample, which changes sign as a function of frequency and temperature [34].

The behavior of the DC phase on sudden or gradual removal of the applied electric field depends on the stage at which it is turned off. For example, following the removal of a sufficiently high field to form macroscopic conglomerate domains $\boldsymbol{E} > \boldsymbol{E}_{\mathrm{th1}}$, no change is observed either in the size or shape of the domains [Figs. 9(a) and 9(b)]. This implies that once the domains are formed, they remain stable even after turning the field off. However, if the field is turned off after the achiral state is reached, $\boldsymbol{E} > \boldsymbol{E}_{\mathrm{th3}}$, tiny domains of opposite handedness start to nucleate. However large area domains of one handedness (left) are always obtained [Figs. 9(c) and 9(d)]. It is also interesting to note that above $\boldsymbol{E} > \boldsymbol{E}_{\mathrm{th2}}$, i.e., once the opposite-handed domains become visible, removal of the field or changing the temperature of the DC phase does not return the sample to the original texture of a fresh cell. Instead, the opposite-handed domains remain visible, even after keeping the cell at $\boldsymbol{E} = 0$ for several hours. To remove these chiral domains, one needs to heat up the cell beyond the DC to N phase transition temperature and then recool to the DC phase. On every heating-cooling sequence, neither the texture of the

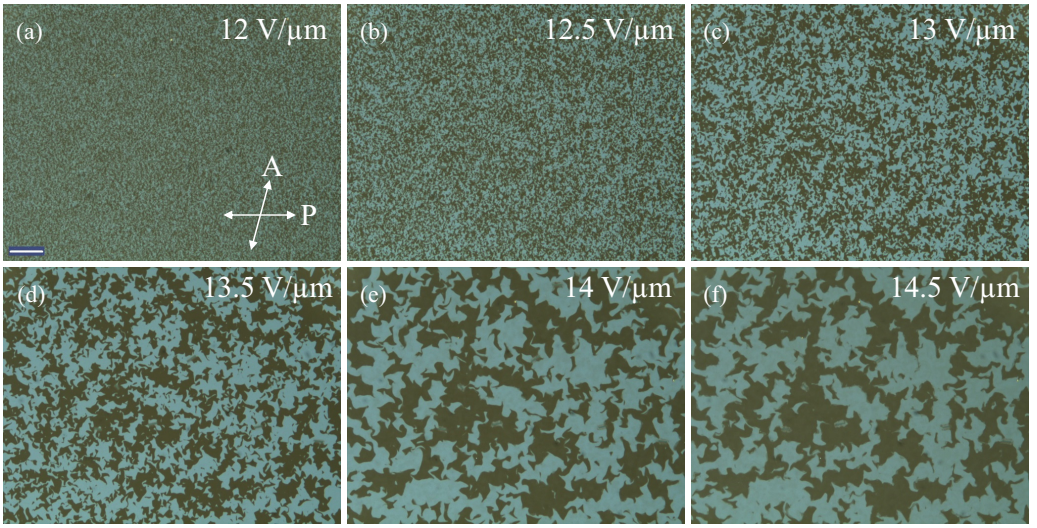

FIG. 7. (Color online) Photomicrographs of electric-field-driven chiral domains for $\boldsymbol{E} > \boldsymbol{E}_{\text{th2}}$ at T–$T_{N\text{-DC}} = -4\,^{\circ}$C. For a given frequency, the domains size increases as the field strength increases. Results are shown for $f = 1$ kHz at (a) 12 V μm^{-1}, (b) 12.5 V μm^{-1}, (c) 13 V μm^{-1}, (d) 13.5 V μm^{-1}, (e) 14 V μm^{-1}, (f) 14.5 V μm^{-1}. Length of the white bar is 100 μm. The orientation of the polarizer P and analyzer A are shown in (a), but apply to each of the figures shown.

DC phase obtained nor the position of the chiral domains was seen to be reproducible and hence is not dictated by the surfaces.

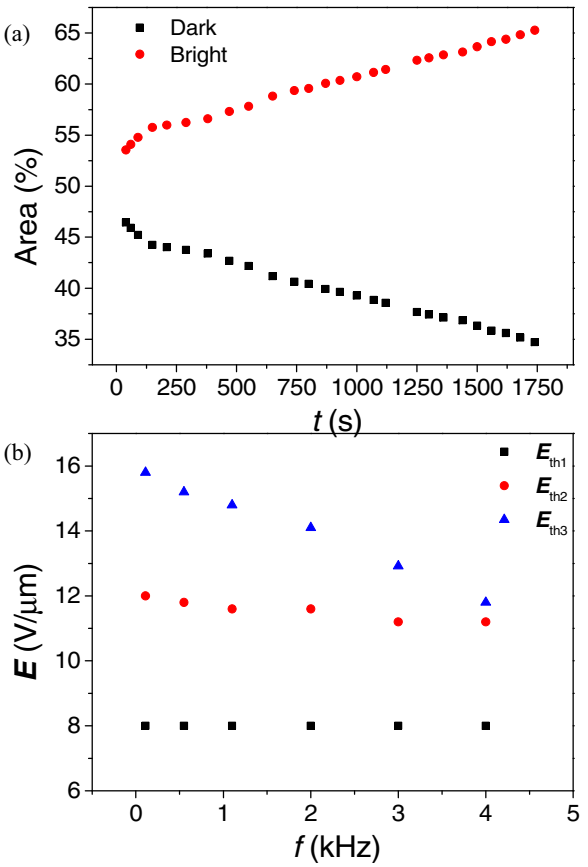

FIG. 8. (Color online) Plot of (a) time dependence of percentage of area occupied by the opposite-handed domains in the field of view of the POM at $\boldsymbol{E} = 14$ V μm^{-1}, $f = 1$ kHz; (b) frequency dependence of the threshold electric fields at T–$T_{N\text{-DC}} = -4\,^{\circ}$C.

2. SAXS

In order to understand the structural reorganization occurring within the DC phase on application of an electric field, small angle x-ray scattering experiments were carried out under high electric fields. Figure 10 shows the behavior of the periodicity, full width half maximum, and amplitude of the diffraction pattern as a function of applied electric field 4 °C below the N-DC phase transition. For a continuous increase in the applied field, the d spacing increases from 30.03 Å ($\theta_C = 27.9^{\circ}$) at $\boldsymbol{E} = 0$ to 30.32 Å ($\theta_C = 26.9^{\circ}$) at $\boldsymbol{E} = 13$ V μm^{-1} ($>\boldsymbol{E}_{\text{th2}}$). For higher electric fields, a slight decrease in the d values is observed corresponding to 30.26 Å at $\boldsymbol{E} = 15$ V μm^{-1} ($\sim E_{\text{th3}}$) ($\theta_C = 27.1^{\circ}$). The FWHM follows the d-spacing trend (increasing from 0.3 to 0.36 nm and

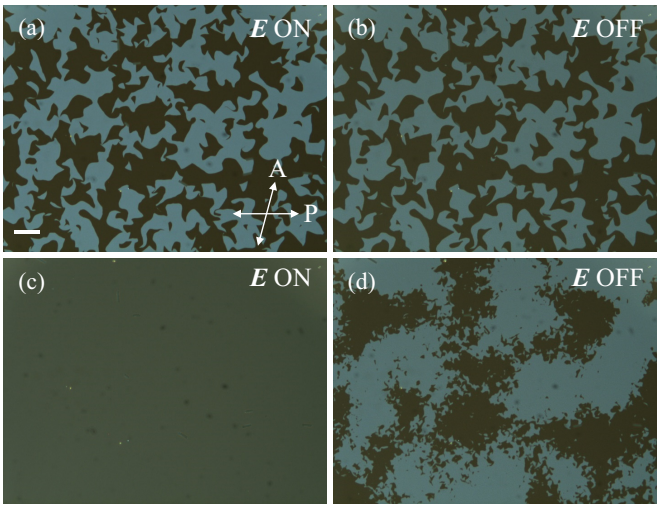

FIG. 9. (Color online) Dynamics of the chiral domains on turning the field off. On and Off states when the field (a,b) $\boldsymbol{E}_{\text{th2}} < \boldsymbol{E} < \boldsymbol{E}_{\text{th3}}$ and (c,d) $\boldsymbol{E} > \boldsymbol{E}_{\text{th3}}$ is applied across the device. Length of the white bar is 100 μm, which is applicable to all of the photographs.

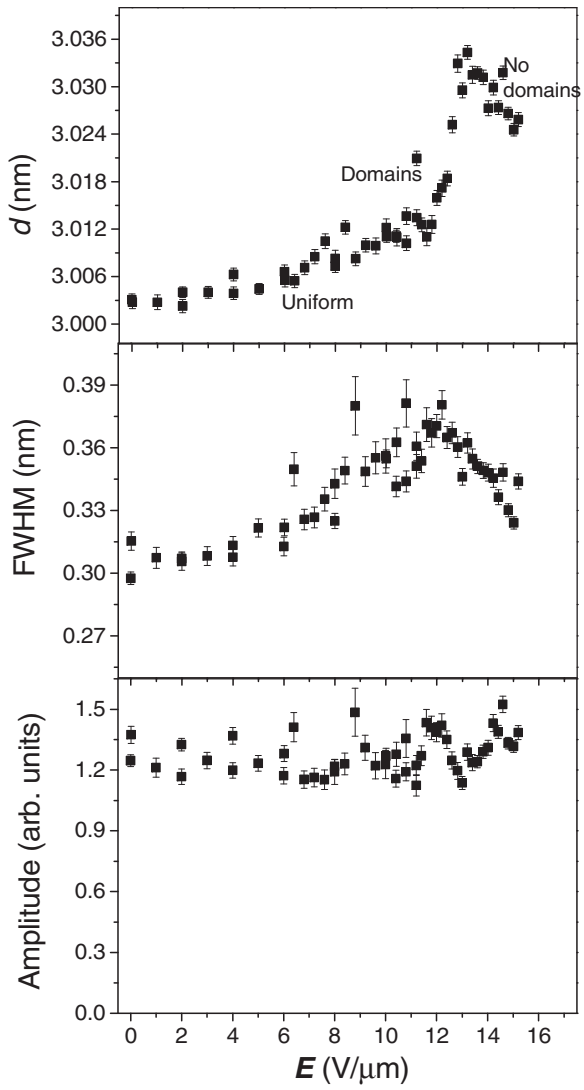

FIG. 10. Electric-field dependence of (a) periodicity, d, (b) FWHM, and (c) amplitude, calculated from the 2D diffraction pattern at $T-T_{N\text{-DC}} = -4\,^{\circ}\text{C}$. Cell gap $= 5\,\mu$m. The threshold fields corresponding to textural changes are $\boldsymbol{E}_{\text{th1}} \sim 8\,\text{V}\,\mu\text{m}^{-1}$ and $\boldsymbol{E}_{\text{th2}} \sim 12\,V\,\mu\text{m}^{-1}$.

then decreasing to 0.33 nm), although the amplitude of the diffraction peak remains constant throughout the experiment.

3. Dielectric spectroscopy

Information pertaining to the molecular reorganization in the DC phase under the applied electric field was further investigated by measuring the field dependence of the dielectric permittivity, ε'. The experiment was carried out with simultaneous optical observation using a polarizing microscope in order to correlate the field-induced optical changes with those of the permittivity. Figure 5(d) shows a typical electric-field dependence of the average dielectric permittivity, ε', at 1 kHz and $T-T_{N\text{-DC}} = -4\,^{\circ}\text{C}$. On increasing the applied electric field, ε' increases slowly from $\varepsilon' \sim 26$ to $\varepsilon' \sim 29$ at $\boldsymbol{E} \sim 8\,\text{V}\,\mu\text{m}^{-1}$ $(=\boldsymbol{E}_{\text{th1}})$. Further increase in the field induces a considerable increase of the permittivity ε', which saturates at $\varepsilon' \sim 58$ for $\boldsymbol{E} > 12\,\text{V}\,\mu\text{m}^{-1}$ (i.e., $\boldsymbol{E} > \boldsymbol{E}_{\text{th2}}$). The temperature dependence of the dielectric permittivity at 1 kHz for various electric fields is given in Fig. 10(e). Clearly, the large increase in ε' observed at the N-DC phase transition is strongly field dependent.

4. Calculation of molecular polarizability

The molecular polarizability of OC12-Ph-ODBP-Ph-C5 was calculated by quantum mechanical calculations using the GAUSSIAN 09 package [45]. The calculations were performed by density functional theory (DFT) employing the combination of the Becke (3-parameter)–Lee–Yang–Parr (B3LYP) hybrid functional and the 6-31$g(d,p)$ basis set. The ratio of polarizability anisotropy to the average, $\frac{\Delta\alpha}{\bar{\alpha}}[\Delta\alpha = \alpha_{\parallel} - \alpha_{\perp}, \bar{\alpha} = \frac{1}{3}(\alpha_{\parallel} + 2\alpha_{\perp})]$ obtained from the DFT calculations is ~0.47, which is within 2% of the value calculated from the refractive indices data obtained in the nematic phase in Ref. [35]. The calculations also predict high biaxiality of the polarizability tensor with $\frac{\partial\alpha}{\bar{\alpha}} = +0.25$ ($\partial\alpha = \alpha_2 - \alpha_1$, α_1 being along the shortest molecular axis). Assuming that the phase biaxiality parameter C for the SmCP phase is high then we would expect the optical biaxiality to be of the order of half the uniaxial nematic birefringence ($\partial\alpha \approx 0.4$).

V. DISCUSSION

A. Two DC phase regimes

The 2D diffraction pattern for the DC phase of OC12-Ph-ODBP-Ph-C5 liquid crystal exhibits a diffuse ring which, close to the N-DC phase transition, corresponds to a periodicity of less than the molecular length. This observation agrees with the generally accepted model of the DC phase, i.e., that the phase consists of a SmCP structure with a short-range interlayer correlation length in which the layers curve continuously in space to form an optically isotropic sponge-like structure. From the SAXS results for OC12-Ph-ODBP-Ph-C5, it is clear that there are two distinct regimes in the DC phase (Fig. 4). In the first regime (higher temperature DC1) the periodicity decreases slightly (0.5% of that close to the N-DC phase transition) and the FWHM and the amplitude of the peak remain constant on reducing the temperature. Such behavior is similar to that observed in the SmC phase of both calamitic and bent-core liquid crystals [46] below a first order N–SmC phase transition, when the cone angle increases only slightly with decreasing temperature. However, surprisingly, on further reducing the temperature of the DC phase, below $T-T_{N\text{-DC}} = -35\,^{\circ}\text{C}$ a second DC phase regime is observed (DC2) in which the periodicity, FWHM, and the amplitude of the diffraction pattern continuously increase with reducing temperature. An increase in the periodicity, consistent with a decrease in the molecular tilt angle, on decreasing the temperature, as seen in the DC2 regime, has not been observed previously in the DC phase of other BCLCs. The change in the periodicity occurs concurrently with an increase in the scattering amplitude, suggesting that the aliphatic chains are more ordered within the layers at lower temperatures. In addition to these changes, an increase in FWHM suggests that the correlation length within the DC structure decreases while the more crystalline alkyl chains are accommodated. In other words, the arrangement becomes even spongier at lower

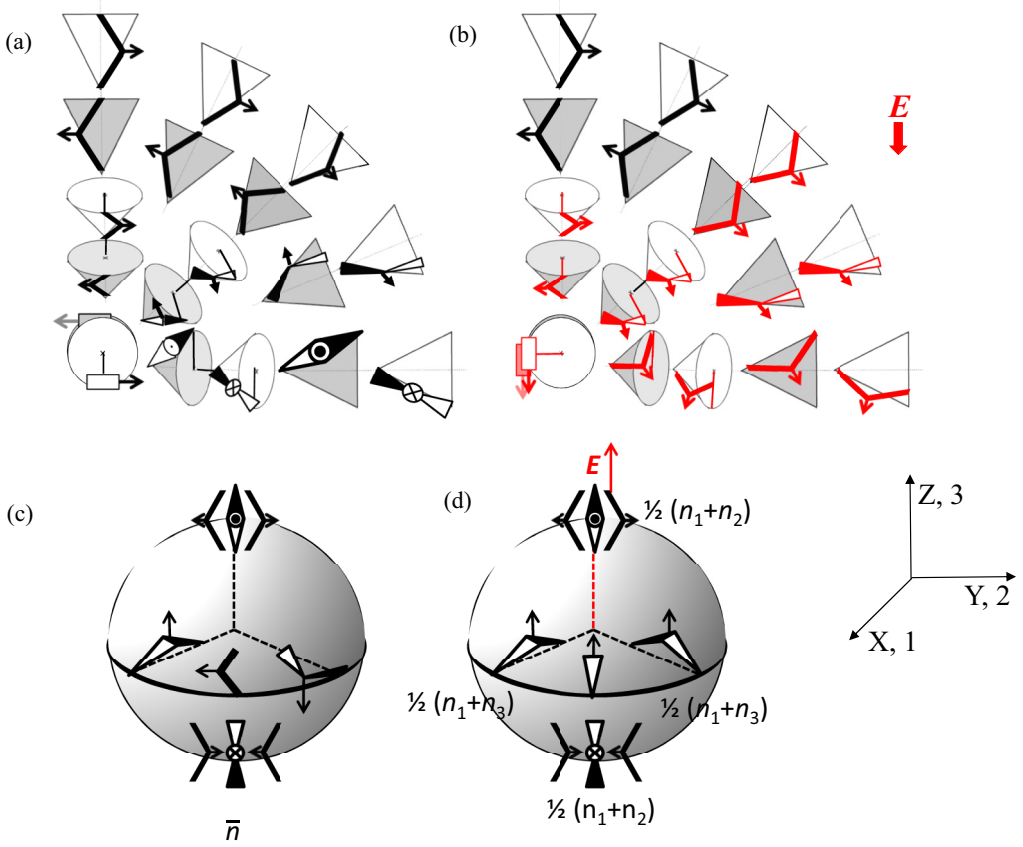

FIG. 11. (Color online) Cartoon representation of the molecular arrangement and their tilt cone in the DC phase, in one quadrant, assuming the sphere model for simplicity. (a) Sm$C_A P_A$ type organization without electric field; (b) Sm$C_A P_F$ type organization when electric field applied. Molecular arrangement on a sphere in (c) the ground state of the DC phase and (d) in the presence of electric field.

temperatures, in contrast to what might be expected normally. Also, at very low temperatures just before the crystalline transition, the observed d spacing is slightly higher than the calculated molecular length. From the temperature dependence of the electric permittivity and current response measurements (double current peak per half cycle of the applied wave form) [29] it is known that the ground state of the DC phase has an antiferroelectric arrangement (Sm$C_A P_A$) within the layers [Fig. 11(a)]. However, unlike the DC phase of other bent-core liquid crystals, no spontaneous chiral domains are visible in the ground state at any temperature corresponding to the DC phase for this compound. This implies that in the ground state the domains must be smaller than the wavelength of the visible light. The SAXS results indicate that the DC2 has similar molecular arrangement (Sm$C_A P_A$-type) within a layer to that of DC1.

B. E-field-induced changes and molecular reorientation mechanisms

When an electric field is applied to the DC phase of OC12-Ph-ODBP-Ph-C5, for fields between $\boldsymbol{E}_{\text{th1}}$ and $\boldsymbol{E}_{\text{th2}}$, the dipoles align parallel to the applied electric field due to strong molecular biaxiality (Sec. IV B 3). This gives rise to an increase in the size of the conglomerate domains, which become visible above $\boldsymbol{E}_{\text{th2}}$. The argument is supported by a small increase in the dielectric permittivity observed during these changes [Fig. 5(c)] and the increases in the strength of a C-C stretching peak at 1589 cm^{-1}, observed in the Raman scattering experiments [29]. Further, the chiral domains continue to grow with further field increase until an enantiomeric state is achieved. The handedness of this enantiomeric state seems to be a fundamental characteristic of the material, being independent of sample related factors, which may be explained by considering the circular dichroic (CD) spectroscopy data [29]. The ground state of the DC phase of the bent-core liquid crystal shows positive CD values, implying that the ground state has a bias towards one handedness and it is this *same handedness* that becomes dominant under a high electric field. Considering the fact that the bent-core molecule exhibits chiral conformers, it is possible that the electric field aids improving the packing of similar conformers leading to a bias towards one handedness over the other. The behavior of bias towards the growth of one handedness has been observed in another system where the dark conglomerate phase is induced by applying an electric field to a tilted columnar structure [43].

Once the enantiomeric state is reached, further increase of the electric field leads to an achiral state. This has been explained to be due to a switching from the antiferroelectric arrangement of the layers to the ferroelectric arrangement (switching between Sm$C_A P_A$ to Sm$C_A P_F$) [Figs. 11(a) and 11(b)] [29]. This switching implies that the collective switching due to the polarity of the phase occurs

by the rotation of the molecules around their long axes and not around the tilt cone [47], which is in line with the small change (1%) in periodicity observed by SAXS. The small increase in the periodicity observed by SAXS measured at $T - T_{N\text{-DC}} = -4\,^{\circ}\text{C}$, with electric field applied, can also be explained considering the presence of collective motion close to the N-DC phase transition (Fig. 5). The increase in the periodicity is due to the changes in the cone angle with applied field, with a slight decrease in the average tilt implied.

Further agreement to the switching between Sm$C_A P_A$ to Sm$C_A P_F$ comes from the electrical measurements. There is a strong increase in the electric permittivity corresponding to the onset of polarity, and this is seen from the current response, which shows a double peak for $\boldsymbol{E} < \boldsymbol{E}_{\text{th3}}$ that becomes a single peak at higher electric fields. It has been shown that bent-core molecular layers favor the saddle-splay curvature only when the tilt directions of the top and bottom molecular arms of adjacent layers are coplanar [5]. This criterion is satisfied in the bilayer systems of chiral Sm$C_S P_F$ and Sm$C_A P_A$ phases as shown by the shading in Fig. 1(b), but not for the racemic Sm$C_S P_A$ and Sm$C_A P_F$ structures. For simplicity of visualization let us represent the spontaneously saddle-splayed layers of the DC phase as a sphere, where the layer normal is pointing outward at each point and is perpendicular to the surface of the sphere. This is represented in Fig. 11(c) for the ground state of the DC phase, where at the "poles" the average orientation of molecules is vertical (the polarization direction is horizontal) and at the "equator" the average orientation of the molecules is horizontal (the polarization direction is vertical). A low electric field is insufficient to cause any layer orientation, which remain isotropically distributed. In this situation, the molecules at the equator align along the field direction whereas those at the poles do not reorient since the field is normal to the polarization. The director at the poles is surrounded in all directions by layers curving away and any field-induced elastic distortion is balanced at the pole on all sides, and the poles remain unchanged for even high fields. Such a reorganization induced by the applied electric-field coupling to the in-layer polarization produces an optic axis parallel to the field direction and the total refractive index $[=\bar{n} - \frac{1}{6}(n_2 - n_1)]$ will be lower than the average refractive index, $\bar{n}$ of the undistorted system, if the local optical biaxiality of the DC phase is positive. Such a structure can explain the unusual decrease in the average refractive index observed in the system on increasing electric field. The magnitude of the change in refractive index measured in Ref. [29] is about 0.045, predicting that the local optical biaxiality of the DC phase $n_2 - n_1$ is about 0.15 compared to the uniaxial birefringence extrapolated from the nematic phase of 0.23. This suggests that the biaxial order parameter of the DC phase is high. Even so, given that molecular modeling suggests that the molecular polarizability biaxiality $\partial\alpha$ is almost half that of the uniaxial molecular polarizability $\Delta\alpha$ it is possible that there is also some layer reorientation that increases the effect.

Furthermore the possibility that the electric field inducing the lower temperature DC phase is ruled out by the fact that the change in the periodicity, FWHM, and the amplitude of the diffraction pattern obtained for temperature dependence do not correspond to that estimated by extrapolating the field-induced changes to infinite electric fields. A study of the nature of the elastic constants in the nematic phase of our material has shown that this mesogen possesses relatively low splay, twist, and bend elastic constants ($K_{11} = 8\,\text{pN}$, $K_{22} = 1\,\text{pN}$, $K_{33} = 3\,\text{pN}$ close to the N–DC phase transition) [35,36]. The standard theoretical elastic approach predicts that the saddle-splay elastic constant $K_{24} \leqslant 2K_{11} + K_{22}$ or $K_{24} < K_{22}$, whichever is smaller [48–50]. Therefore, the absence of a field-induced complete deformation of the sponge-like structure of the DC phase of our material could be because of the possibility of a more highly negative K_{24} elastic constant in this material. Alternatively, we propose that the sponge-like texture must be retained because of the lack of electrical torque acting at the poles of the structure. The quiescent Sm$C_A P_A$ state can transform to either a chiral lamellar Sm$C_S P_F$ through collective motion about the layer normal or to the achiral sponge-like structure of the Sm$C_A P_F$ phase, through a rotation about the long molecular axes, as shown in Fig. 2. However, no switching of the pole regions occurs, leading to the retention of local points of Sm$C_A P_A$ with the sponge structure throughout the system. This prevents layer reorientation to the simple lamellar phases and forces the material to undergo the more frustrated transition to the Sm$C_A P_F$ phase, and the reduction of chirality through domain growth. The frustration of the phase is evident from the increased distribution of layers in the FWHM of the x-ray diffraction.

VI. CONCLUSIONS

A detailed investigation is reported on the phenomenon of chiral symmetry breaking in an achiral bent-core liquid crystal, when an electric field is applied to the liquid crystal in its DC phase and on the unusual nature of this DC phase. The nature and dynamics of the field-induced transformations and physical reasons responsible are discussed in detail. Some of the major differences between the DC phase commonly known in the literature and that exhibited by OC12-Ph-ODBP-Ph-C5 liquid crystal are as follows:

(i) In the DC phase of OC12-Ph-ODBP-Ph-C5 liquid crystal, there are two distinct regimes—a higher temperature one for which the periodicity decreases slightly and a lower temperature regime for which it increases considerably.

(ii) OC12-Ph-ODBP-Ph-C5 exhibits no macroscopic conglomerates of chiral domains in the ground state.

(iii) In the presence of an electric field, the DC phase exhibits a unique set of field-induced states.

The changes involve fields that are temperature and frequency dependent and the phenomena are observed irrespective of device thickness, geometry, or the alignment layer. The electro-optical phenomena are simultaneous with a small increase in d spacing and a large increase in the average dielectric permittivity of the system. The experiments suggest that the electric field causes a rearrangement within the nanostructure of the DC phase, without gross structural reorganization: the sponge-like structure is retained throughout. We have presented a model for the field-induced rearrangement that is consistent with the experimental data; the model is characterized by a reorganization of the sponge-like structure from an anticlinic antiferroelectric organization to an anticlinic ferroelectric order without any gross structural changes and

keeping the sponge-like structure of the DC intact because of the network of unswitching regions throughout the structure.

Interestingly, we investigated a number of similar compounds for the field-induced behavior and found that the unusual electric-field-induced transformations described in this paper occur only in the bent-core material that possesses the combination of alkyl and alkoxy terminal chains. Some of the homologues of the same oxadiazole bent-core series, which possess alkyl terminal chains on both sides, also exhibit the DC phase. However, the DC phase in those materials clearly shows optically active macroscopic domains in the ground state. A detailed investigation on this will be published elsewhere.

The DC phase of OC12-Ph-ODBP-Ph-C5 liquid crystal is an interesting system as the DC phase exists below a nematic phase and exists over a wide range of temperature. This uniquely offers a great advantage in understanding the mesophase behavior because many physical properties can be measured in the nematic phase and the behavior extrapolated to lower temperatures and the DC phase. It could be used as a model system to understand chiral domain growth, coarsening, and scaling hypothesis and also to investigate generating and controlling chiral symmetry breaking in achiral condensed matter systems. Chirality tuning in an achiral system by applying electric field of different strengths and frequencies is important for the applications in chiro-optical and nonlinear optics and in optoelectronic devices.

ACKNOWLEDGMENTS

M.N. thanks the Royal Commission for the Exhibition of 1851 for support through a research fellowship. J.C.J. wishes to thank the EPSRC for the provision of support through an EPSRC Fellowship in Advanced Manufacturing (Grant No. EP/L015188/1). V.P. and H.F.G. thank the EPSRC, UK, for funding (Grants No. EP/G023093/1 and No. EP/D055261/1). The authors also acknowledge funding from the Dutch Science Foundation (NWO) and Flemish Research Foundation (FWO) for access to the x-ray facilities. V. Görtz, Lancaster and J. W. Goodby, York are thanked for providing the liquid crystal.

[1] M. B. Ros, J. L. Serrano, M. R. de la Fuente, and C. L. Folcia, J. Mater. Chem. **15**, 5093 (2005).
[2] H. Takezoe and Y. Takanishi, Jpn. J. Appl. Phys. **45**, 597 (2006).
[3] R. Reddy and C. Tschierske, J. Mater. Chem. **16**, 907 (2006).
[4] H. Niwano, M. Nakata, J. Thisayukta, D. R. Link, H. Takezoe, and J. Watanabe, J. Phys. Chem. B **108**, 14889 (2004).
[5] L. E. Hough, H. T. Jung, D. Krüerke, M. S. Heberling, M. Nakata, C. D. Jones, D. Chen, D. R. Link, J. Zasadzinski, G. Heppke, J. P. Rabe, W. Stocker, E. Körblova, D. M. Walba, M. A. Glaser, and N. A. Clark, Science **325**, 456 (2009).
[6] D. M. Walba, L. Eshdat, E. Körblova, and R. K. Shoemaker, Cryst. Growth Des. **5**, 2091 (2005).
[7] G. Dantlgraber, A. Eremin, S. Diele, A. Hauser, H. Kresse, G. Pelzl, and C. Tschierske, Angew. Chem. Int. Ed. **41**, 2408 (2002).
[8] G. Dantlgraber, S. Diele, and C. Tschierske, Chem. Commun. 2768 (2002).
[9] J. Thisayukta, Y. Nakeyama, S. Kawauchi, H. Takezoe, and J. Watanabe, J. Am. Chem. Soc. **122**, 7441 (2000).
[10] J. Ortega, C. L. Folcia, J. Etxebarria, N. Gimeno, and M. B. Ros, Phys. Rev. E **68**, 011707 (2003).
[11] Y. Zhang, U. Baumeister, C. Tschierske, M. J. O'Callaghan, and C. Walker, Chem. Mater. **22**, 2869 (2010).
[12] W. Weissflog, M. W. Schröder, S. Diele, and G. Pelzl, Adv. Mater. **15**, 630 (2003).
[13] I. Wirth, S. Diele, A. Eremin, G. Pelzl, S. Grande, L. Kovalenko, N. Pancenko, and W. Weissflog, J. Mater. Chem. **11**, 1642 (2001).
[14] C. Zhang, N. Diorio, O. D. Lavrentovich, and A. Jákli, Nat. Commun. **5**, 3302 (2015).
[15] D. Chen, R. Shao, J. E. Maclennan, M. A. Glaser, E. Korblova, D. M. Walba, N. Gimeno, M. B. Ros, and N. A. Clark, Liq. Cryst. **40**, 1730 (2013).
[16] H. Ocak, B. B. Eran, M. Prehm, and C. Tschierkse, Soft Matter **8**, 7773 (2012).
[17] D. R. Link, G. Natale, R. Shao, J. E. Maclennan, N. A. Clark, E. Körblova, and D. M. Walba, Science **278**, 1924 (1997).
[18] V. Görtz, C. D. Southern, N. W. Roberts, H. F. Gleeson, and J. W. Goodby, Soft Matter **5**, 463 (2009).
[19] F. Yan, C. A. Hixson, and D. J. Earl, Soft Matter **5**, 4477 (2009).
[20] S. Kawauchi, S.-W. Choi, K. Fukuda, K. Kishikawa, J. Watanabe, and H. Takezoe, Chem. Lett. **36**, 750 (2007).
[21] H. Kurosu, M. Kawasaki, M. Hirose, M. Yamada, S. Kang, J. Thisayukta, M. Sone, and H. Takezoe, J. Phys. Chem. A **108**, 4674 (2004).
[22] D. J. Earl, M. A. Osipov, H. Takezoe, Y. Takanishi, and M. R. Wilson, Phys. Rev. E **71**, 021706 (2005).
[23] H. Takezoe, Top. Curr. Chem. **318**, 303 (2012).
[24] H. S. Jeong, S. Tanaka, D. K. Yoon, S.-W. Choi, Y. H. Kim, S. Kawauchi, F. Araoka, H. Takezoe, and H.-T. Jung, J. Am. Chem. Soc. **131**, 15055 (2009).
[25] C. Keith, R. A. Reddy, M. Prehm, U. Baumeister, H. Kresse, J. L. Chao, H. Hahn, H. Lang, and C. Tschierske, Chem. Eur. J. **13**, 2556 (2007).
[26] G. Porte, J. Appell, P. Bassereau, J. Marignan, M. Skouri, I. Billard, and M. Delsanti, Phys. A (Amsterdam, Neth.) **176**, 168 (1991).
[27] S. K. Lee, L. Shi, M. Tokita, H. Takezoe, and J. Watanabe, J. Phys. Chem. B Lett. **111**, 8698 (2007).
[28] J. Ortega, C. L. Folcia, J. Etxebarria, J. Martínez-Perdiguero, J. A. Gallastegui, P. Ferrer, N. Gimeno, and M. Blanca Ros, Phys. Rev. E **84**, 021707 (2011).
[29] M. Nagaraj, K. Usami, Z. Zhang, V. Görtz, J. W. Goodby, and H. F. Gleeson, Liq. Cryst. **41**, 800 (2014).
[30] L. S Matkin, S. J. Watson, H. F. Gleeson, R. Pindak, J. Pitney, P. M. Johnson, C. C. Huang, P. Barois, A.-M. Levelut, G. Srajer, J. Pollmann, J. W. Goodby, and M. Hird, Phys. Rev. E **64**, 021705, 2001.
[31] H. F. Gleeson, G. K. Bryant, and A. S. Morse, Mol. Cryst. Liq. Cryst. **362**, 203 (2001).

[32] T. C. Huang, H. Toraya, T. N. Blanton, and Y. Wu, J. Appl. Cryst. **26**, 180 (1993).
[33] C. D. Southern, P. D. Brimicombe, S. D. Siemianowski, S. Jaradat, N. Roberts, V. Görtz, J. W. Goodby, and H. F. Gleeson, Europhys. Lett. **82**, 56001 (2008).
[34] S. Kaur, A. Belaissaoui, J. W. Goodby, V. Görtz, and H. F. Gleeson, Phys. Rev. E **83**, 041704 (2011).
[35] S. Kaur, J. Addis, C. Greco, A. Ferrarini, V. Görtz, J. W. Goodby, and H. F. Gleeson, Phys. Rev. E **86**, 041703 (2012).
[36] S. Kaur, H. Liu, J. Addis, C. Greco, A. Ferrarini, V. Görtz, J. W. Goodby, and H. F. Gleeson, J. Mater. Chem. C **1**, 6667 (2013).
[37] H. F. Gleeson, S. Kaur, V. Görtz, A. Belaissaoui, S. Cowling, and J. W. Goodby, Chem. Phys. Chem. **15**, 1251 (2014).
[38] M. Nagaraj, V. Görtz, J. W. Goodby, and H. F. Gleeson, Appl. Phys. Lett. **104**, 021903 (2014).
[39] H. E. Milton, M. Nagaraj, S. Kaur, P. B. Morgan, J. C. Jones, and H. F. Gleeson, Appl. Opt. **53**, 7278 (2014).
[40] S. Kaur, V. P. Panov, C. Greco, A. Ferrarini, V. Görtz, J. W. Goodby, and H. F. Gleeson, Appl. Phys. Lett. **105**, 223505 (2014).
[41] C. Southern, Ph.D. thesis, University of Manchester, 2009, p. 95.
[42] A. Eremin, H. Nádasi, G. Pelzl, S. Diele, H. Kresse, W. Weissflog, and S. Grande, Phys. Chem. Chem. Phys. **6**, 1290 (2004).
[43] G. B. Deepa and R. Pratibha, Phys. Rev. E **89**, 042504 (2014).
[44] M. Nagaraj, J. C. Jones and H. F. Gleeson (unpublished).
[45] GAUSSIAN 09, Revision B.01 (Gaussian, Inc. Wallingford, CT, 2010).
[46] S. Kumar, in *Handbook of Liquid Crystals*, edited by J. W. Goodby, P. J. Collings, T. Kato, C. Tschierske, H. F. Gleeson, and P. Raynes (Wiley-VCH, Weinheim, 2014), Vol. 1, p. 326.
[47] M. Nakata, R.-F. Shao, J. E. Maclennan, W. Weissflog, and N. A. Clark, Phys. Rev. Lett. **96**, 067802 (2006).
[48] R. D. Polak, G. P. Crawford, B. C. Kostival, J. W. Doane, and S. Žumer, Phys. Rev. E **49**, R978 (1994).
[49] V. M. Pergamenshchik and S. Žumer, Phys. Rev. E **59**, R2531 (1999).
[50] G. Barbero and V. M. Pergamenshchik, Phys. Rev. E **66**, 051706 (2002).